Journal of Molecular Liquids 360 (2022) 119593

Contents lists available at ScienceDirect

Journal of Molecular Liquids

journal homepage: www.elsevier.com/locate/molliq

NiO nanowire-containing heat transfer nanofluids for CSP plants: Experiments and simulations to promote their application

Desireé M. De los Santos, Iván Carrillo-Berdugo *, Alejandro Domínguez-Núñez, Juan Antonio Poce-Fatou, David Zorrilla, Javier Navas *

Departamento de Química Física, Facultad de Ciencias, Universidad de Cádiz, E-11510 Puerto Real (Cádiz), Spain

ARTICLE INFO

Article history:
Received 9 March 2022
Revised 30 May 2022
Accepted 7 June 2022
Available online 9 June 2022

Keywords:
Nanofluids
Concentrating solar power
Thermal conductivity
Specific heat
Volumetric absorption
Molecular dynamics

ABSTRACT

Concentrating solar power (CSP) is considered a clean, renewable and sustainable energy with a significant potential to become an alternative to polluting fossil fuel-based technologies. Among CSP collectors, parabolic-trough collectors (PTC) are the most mature technology, representing nearly 90% of the currently installed collectors in CSP plants worldwide. In this technology, a heat transfer fluid (HTF) carries the thermal energy absorbed to a power block to produce electricity. Improving the thermal properties of the conventional HTF could lead to an improvement of the efficiency of CSP plants. In this sense, the use of nanofluids as the HTF in these plants can be a promising choice. Here, polycrystalline NiO nanowire-containing nanofluids have been prepared using the conventional HTF used in CSP plants as the base fluid; that is, the eutectic and azeotropic mixture of biphenyl (26.5%) and diphenyl oxide (73.5%). The stability, rheological and thermal properties have been characterized, and an analysis of the performance of the nanofluids prepared in standard and volumetric absorbers have been carried out. The overall CSP system performance can be increased up to 34.8% using the nanofluid in a surface collector or up to 34.3% using the nanofluid in a volumetric collector, which are better than the predicted 28.5% using the conventional HTF in a standard surface collector, thanks to the improvements in thermal properties, both specific heat and thermal conductivity. Finally, from molecular dynamics simulations we determined that the mean free path of thermal vibrations is longer for monocrystalline NiO nanowires. Thus, the development of strategies for obtaining this kind of nanostructures is of great interest because they can further improve the efficiency of these nanofluids.

1. Introduction

The current social and economic context encourages the development and increasing use of renewable energy technologies. In this paper we pay attention to the concentrating solar power (CSP) technology [1] based on parabolic-trough collectors (PTC) [2], *i.e.*, curved mirrors (with a parabola-shaped cross section) that focus solar radiation on a pipe containing a heat transfer fluid (HTF) that discharges its energy in a thermodynamic cycle to obtain electricity. The selection of the HTF in these technologies is key as it influences the efficiency of the plant and the type of energy storage device to be attached. There are plants that directly use steam as the HTF. These are known as Direct Steam Generation (DSG) systems. They provide higher yields because the HTF can reach much higher temperatures. The main drawback is that they require sophisticated control strategies and technologies that increase production costs [3]. Another option is the use of molten salts, mainly sodium–potassium nitrates. They offer thermophysical properties and stability that facilitate high yields. However, these species have high melting points, which means that the molten salt freezing phenomenon [4] must be avoided, especially when the plant is not active.

Good *et al.* have tested the use of pressurized air as HTF, an option that can be varied by substituting other gases for air. The main advantages of using pressurized gases are their wide range of operating temperatures, abundance and environment-friendly nature. However, this choice needs to overcome major challenges such as low heat transfer coefficient and high pumping power consumption [5]. Synthetic thermal oils are also commonly used as HTFs in PTC systems. Syltherm 800, Therminol VP-1 or Dowtherm A [2,6–10] are some of the most widely known commercial HTFs. Dowtherm A and Therminol VP-1 are the eutectic and azeotropic mixture of biphenyl (26.5%) and diphenyl oxide (73.5%), and they can operate in liquid phase up to 673 K. As they are quasi-

* Corresponding authors.
E-mail addresses: ivan.carrillo@uca.es (I. Carrillo-Berdugo), javier.navas@uca.es (J. Navas).

https://doi.org/10.1016/j.molliq.2022.119593
0167-7322/

transparent mixtures, the receiver or absorption tube is dark-coloured in order to achieve maximum absorption of the solar irradiation and a reduction in heat losses.

One way to improve these systems is to replace the HTF with a nanofluid; *i.e.,* a suspension of nanoparticles in the HTF itself. The selection of the base fluid is of great importance since the interaction between its molecules, surfactant species and nanoparticles are key to obtain a nanofluid with good stability and improved thermal properties (mainly thermal conductivity and specific heat) or even to obtain coloured nanofluids to avoid the need for dark-coloured pipes in CSP plants. In our case, the selection of the base fluid has been conditioned by the idea of having a nanofluid whose use would minimally alter the working conditions of the CSP-PTC plants (see Fig. 1). Thus, the use of the eutectic and azeotropic mixture of biphenyl and diphenyl oxide (which is the most widely used HTF in CSP-PTC plants) as a base fluid is considered.

We decided to add NiO nanoparticles to this base fluid, which were stabilised with the surfactant Triton X-100. Nanofluids containing NiO nanoparticles are useful in several thermal processes, for example, their use in base fluids with lubricant function enhances the ability to resist thermal decomposition [11] and when used to obtain nanofluids in distilled water, they improve the energy transfer properties in heat exchangers [12]. NiO nanofluids have been previously studied, from experimental and theoretical perspectives, in our own laboratories in systems stabilised with various surfactants in order to be used in PTCs [13,14]. In all these applications, the nanofluids consisted of NiO nanoparticles. We now report the research carried out to improve the absorption of solar energy, as well as its discharge in a system that employs nanofluids constituted by NiO nanowires dispersed in the eutectic mixture of biphenyl and diphenyl oxide.

The synthesis of polycrystalline nanowires is straightforward, low-cost and easy to scale up [15]. We have considered the use of this species to analyse various working hypotheses: (i) the suspension of NiO nanowires in the eutectic mixture should increase the thermal conductivity of the HTF, and moreover, if one-dimensional structures are involved, the morphology should limit the phonon scattering mechanisms and thus lengthen its mean free path, which should result in an additional improvement of the thermal conductivity [16,17]; (ii) obtaining stable nanofluids of this species should result in a product with a high absorption coefficient that could make the current coating of the pipes of PTC unnecessary; and (iii) the thermodynamic improvements of the nanofluid should be reflected in cost reductions both in the production system and in the maintenance of the CSP.

The characterisation of the nanowires we have synthetised shows their polycrystalline character and the presence of a multitude of grain boundaries that affect the enhancement of the thermal conductivity [18]. In this work, we have incorporated a study based on molecular dynamics (MD) to compare the characteristics of the nanofluid obtained with polycrystalline NiO nanowire with those that could have a HTF based on the monocrystalline one. To the best of our knowledge, no references are reported on the synthesis of single-crystal NiO nanowires. Our results support the potential use of NiO polycrystalline nanowires in CSP based on PTC and encourage the development of new strategies to address the synthesis of NiO monocrystalline nanowires.

2. Methodology

2.1. Synthesis and characterisation of NiO nanowires

Reagents. Nickel (II) chloride ($NiCl_2$, purity $\geq$ 99.9%), sodium oxalate ($Na_2C_2O_4$, purity $\geq$ 99.99%), were supplied by Sigma-Aldrich. Ethylene glycol (purity $\leq$ 99.50%), ethanol (purity $\geq$ 99.8%) were supplied by Honeywell Riedel-de Haën.

Synthesis of NiO nanowires. The hydrothermal synthesis procedure reported by Dang et al. [15] was carried out for the obtention of NiO nanowires. First, 3.65 mmol of $NiCl_2$ were dissolved into a 1:2 mixture of deionised water and ethylene glycol. Then, 0.91 mmol of $Na_2C_2O_4$ were added, and the mixture was kept under vigorous stirring for 1 h. After that, the solution was transferred into a Teflon-lined stainless-steel autoclave, and it was heated up to 473 K for 24 h. The product was rinsed three times with both deionised water and ethanol by centrifugation (10000 rpm, 15 min). The product was dried at room temperature for up to 48 h and then annealed at 773 K for 2 h.

Characterisation of NiO nanowires. The morphology and crystalline structure of the as-prepared NiO nanowires, as well as the oxidation state of Ni, were characterised. Morphology was determined by transmission electron microscopy (TEM) using an FEI (Hillsboro, Oregon, US) Talos F200X microscope. The existing crystalline phases were determined by X-ray diffraction (XRD) using a Bruker (Billerica, Massachusetts, US) D8 Advanced A25 DaVinci diffractometer, with monochromatic Cu K_α (8.04 keV) radiation operated at 40 kV and 40 mA. The scan ranges 2θ from 10° to 75°, with a resolution of 0.02°. The chemical state bonding and the oxidation state was analysed by X-ray photoelectron spectroscopy (XPS) using a Kratos Analytical Ltd. (Manchester, UK) Axis UltraDLD spectrometer, with monochromatic Al K_α radiation (1.49 keV) and 20 eV pass energy. The binding energy scale was given with an accuracy of 0.1 eV. Electrostatic charging effects were stabilised. Finally, Fourier-transform infrared (FTIR) spectroscopy, with a Bruker (Billerica, Massachusetts, US) Tensor37 spectrometer, was used to verify the obtention of NiO nanowires and the existence of absorbed species on its surface. The spectra

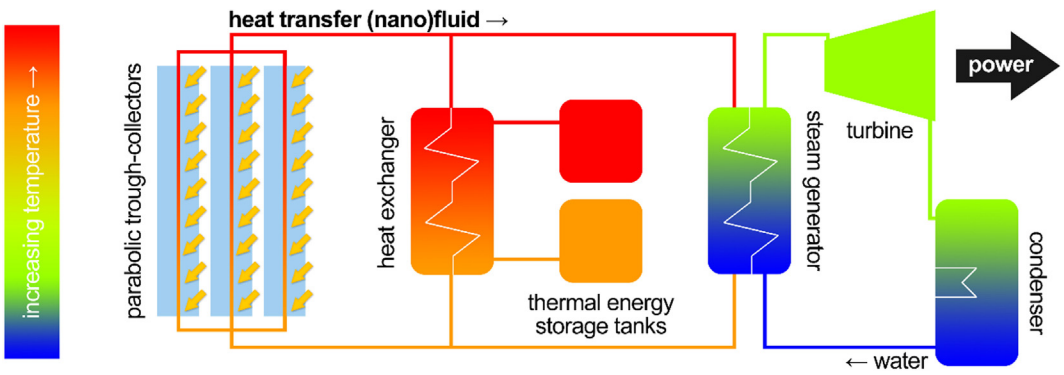

Fig. 1. Scheme of a CSP-PTC plant, highlighting the role of nanofluids in it.

were recorded from 400 cm^{-1} to 4000 cm^{-1} with a resolution of 2 cm^{-1}.

2.2. Preparation and characterisation of NiO nanowire-containing nanofluids

Reagents. The eutectic and azeotropic mixture of biphenyl (BP, $C_{12}H_{10}$, 26.5%) and diphenyl oxide (DPO, $C_{12}H_{10}O$, 73.5%), Dowtherm A, was supplied by The Dow Chemical Company. Triton X-100 (TX-100, surfactant for automatical analysis) was supplied by PanReac AppliChem.

Preparation of nanofluids. NiO nanowire-containing nanofluids were prepared by sonication of the synthesised solid in the host fluid. The host fluid was a 1 wt% TX-100 solution in the base fluid (the mixture of BP and DPO). An initial nanofluid was prepared using 100 ml of the host fluid and the required amount of NiO nanowires to obtain a nanofluid with a mass fraction of NiO equal to 0.01 wt%. The mixture was sonicated using a Sonics & Materials (Newtown, Connecticut, US) Vibra Cell VCX 750 with a 13 mm non-replaceable tip probe at 50% amplitude for 4 h with a 2:4 s on:off pulsation, in a thermostatic bath at 293 K to prevent overheating. After that, aliquots were taken from the stock nanofluid to prepare nanofluids with mass fractions of NiO equal to 0.001 wt% and 0.0001 wt% by addition of host fluid up to 100 ml. Dilutions were sonicated using a PH30 ultrasonic bath supplied by Elmasonic (Singen, Germany), at 80 kHz for 15 min.

Characterisation of nanofluids. The colloidal stability of the nanofluid samples was first analysed. The time evolutions of the particle size and the ζ-potential were studied using the dynamic light scattering (DLS) and the phase analysis light scattering (M3-PALS) techniques, respectively. Both the particle size and the ζ-potential were measured using a Zetasizer Nano ZS system supplied by Malvern Instruments Ltd (Malvern, UK). The aggregation rate was simultaneously analysed using UV–visible spectroscopy. Changes in the extinction coefficient at λ = 500 nm were registered using the OceanOptics (Duiven, The Netherlands) DH2000-Bal halogen lamp and the USB-2000 + spectrometer. All measurements were performed in triplicate, on a daily basis, for 30 days. An additional measurement was performed 200 days after preparation for the assessment of long-term stability.

The applicability of the nanofluid samples as HTFs was also investigated. This is typically done on the basis of a figure-of-merit that is proportional to the heat transfer coefficient, $h \propto \frac{\kappa^a \rho^b C_P^c}{\mu^d \sigma^e}$, where κ is the thermal conductivity, ρ is the density, C_P is the isobaric specific heat, μ is the dynamic viscosity and σ the surface tension. The *a*, *b*, *c*, *d* and *e* exponents are empirical or theoretical constants depending on the geometrical and boundary conditions defined for the application. The exponent *e* is 0 for convection when phase change does not occur, as is the case under study in this work. Therefore, we measured the other four properties of interest of the base fluid and the three nanofluid samples prepared. Density was measured by temperature-controlled pycnometry at 298 K, using a Mettler Toledo (Greifensee, Switzerland) AE 200 analytical balance for the entire gravimetric procedure. Dynamic viscosity was measured using the Discovery HR-10 rheometer supplied by TA Instruments (Milford, Massachusetts, US) with a concentric-cylinder geometry ($Ø_{rotor}$ = 14.0 mm, $Ø_{cup}$ = 15.2 mm) under steady-state shear rate-controlled conditions. Measurements were performed for shear rates between 1 s^{-1} and 100 s^{-1}. Temperature was controlled with an electrically heated concentric jacket. Isobaric specific heat was measured by temperature-modulated differential scanning calorimetry (TM-DSC), using the calorimeter supplied by Netzsch (Selb, Germany), model DSC 214 Polyma. The standard calibration procedure and the temperature program for characterisation have been previously reported [19]. Thermal conductivity was measured by means of the transient hot-bridge (THB-100) technique, whose equipment was supplied by Linseis (Selb, Germany). Nanofluid samples were contained in cylindrical glass vials (up to 2.5 ml) in individually jacketed vessels in an IKA (Oxford, UK) DB 5.2 dry block heater. Dynamic viscosity, specific heat and thermal conductivity values were determined at 298 K, 323 K, 348 K and 373 K.

2.3. Molecular dynamics of NiO nanowire-containing nanofluids

A multiple-model comparison at the MD level-of-theory is the strategy of choice for the study of the effect of crystallinity on the thermal conductivity of nanofluids with NiO nanowires. A total of three different MD models are implicated, one for the base fluid and two for the nanofluid, each with a different structure for NiO nanowires, representing monocrystalline and polycrystalline structures. These representations are compared in Fig. 2. The base fluid model consists of 265 BP molecules and 735 DPO molecules (preserving the eutectic and azeotropic proportion) randomly distributed in the simulation box. A total of at least 1000 molecules in the simulation cell was verified to satisfy the thermodynamic limit condition. The Optimised Potential for Liquid Simulation – All Atom (OPLS-AA) force field [20,21] with parameters from LigParGen [22–24] was considered for bonding and non-bonding interactions between atoms in the base fluid. The nanofluid models consists of 1232 randomly distributed base fluid molecules (also in eutectic and azeotropic proportion) embedding a single nanowire. The monocrystalline nanowire consists of a single-crystal ffc NiO structure with its longitudinal axis developed along the [1 0 0] direction, whereas the polycrystalline nanowire consists of a group of eight fcc NiO cuboctahedra linearly connected by (1 0 0) facets. A semi-ionic approach was considered for the simulation of this metal oxide structures, which is not unprecedent [25], including a Morse potential for covalent contributions between directly neighbouring Ni—O atoms [26–29], and the Coulomb and Lennard-Jones potentials for electrostatic and van der Waals contributions between all others [30]. The Lorentz-Berthelot combining rules are used to parametrise the Lennard-Jones potential for pairwise interactions between odd atoms, including those at the solid–liquid interface. All atoms are explicitly included (no dummy atoms are used).

The Large-scale Atomic/Molecular Massively Parallel Simulator (LAMMPS) [31–33] is the classical MD code of choice. All models were created with Moltemplate [34,35], a molecular builder for LAMMPS. Periodic boundary conditions are imposed in the system. The Verlet integration scheme [36] is used with a timestep of 1 fs. Velocities are rescaled with the Nosé-Hoover thermostat and barostat algorithms [37–40]. Lennard-Jones pairwise interactions are

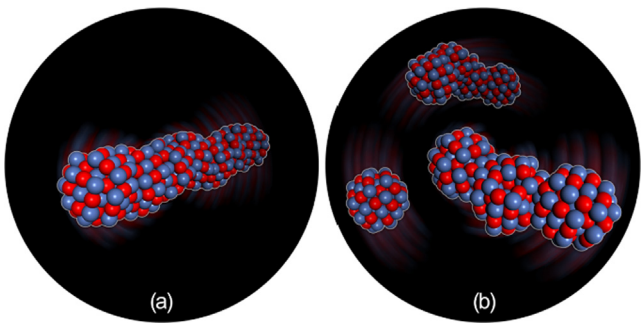

Fig. 2. Monocrystalline (a) and polycrystalline (b) representations of NiO nanowires for MD simulations. These images have been rendered using the actual structures of each nanowire at a given instant of their MD trajectory.

limited to a cut-off distance of 10 Å. The particle–particle particle-mesh (PPPM) summation method was applied to compute long-range electrostatics. A typical MD run requires (i) 0.2 ns in NVE (constant energy, constant volume) for relaxation, (ii) 0.5 ns in NVT (constant temperature, constant volume) for isothermal equilibration, (iii) 2.0 ns in NPT (constant temperature, constant pressure) for isobaric-isothermal equilibration and (iv) 5 ns in NVT for the computation the Green-Kubo thermal conductivity [41,42]. Different runs were carried out with this scheme, at 298 K, 323 K, 348 K and 373 K and 1 atm.

3. Results and discussion

3.1. Characterisation of NiO nanowires

The morphology and nominal particle size of the synthesised NiO nanowires were studied by TEM. The formation of the desired 1D nanostructures is confirmed in view of TEM images in Fig. 2a and 2b. The nominal length of nanowires is determined not to be uniform, as it falls within a range between 600 mm and 1700 nm. The nominal diameter, on the contrary, is similar for all nanowires under observation, and is determined to be about 45 nm on average. It is remarkable, as it can be better seen in Fig. 3b, that nanowires are polycrystalline. They are formed by groups of sintered NiO grains with an average size of about 14 nm. Such architecture is likely a consequence of the formation of NiO crystals with thermodynamically favoured shapes (octahedra, cuboctahedra and cubes) under high temperature conditions, as it happens to be case when the nickel oxalate precursor is calcinated at 773 K to form NiO nanowires.

Fig. 3c shows the diffraction pattern of the as-synthesised NiO nanowires in powder form. Diffraction peaks are observed at 2θ equal to 37.1°, 43.1°, 62.7°, which can be assigned to the diffraction of the (111), (200), and (220) planes, respectively. It matches the reference for NiO cubic phase (JCPDS No. 47–1049) [43]. The patterns do not show evidences of any other crystalline phase of NiO or other species. The average crystallite size of the NiO nanoparticles was estimated to be 15 nm using the Debye-Scherrer equation [44], with a shape factor equal to 0.94 and full width at half maximum (FWHM) of the most intense peak, *i.e.* the reflection of (200) planes. This result is in good agreement with the average diameter estimated from the TEM images. The relative intensity of the peaks associated to the diffraction of (111) and (200) planes suggests a predominant presence of these facets on NiO grains, which is associated to the aforementioned formation of thermodynamically favoured shapes.

The chemical state bonding and the oxidation state of the NiO nanowires were analysed by XPS. The peak assignation is referenced to the signal of adventitious C 1 s at 284.8 eV. Fig. 3e shows the Ni 2p signal. We can observe two peaks at binding energies of 873.2 eV and 856.5 eV, which can be assigned to Ni $2p_{1/2}$ and Ni $2p_{3/2}$, respectively. This large split between the spin–orbit components is unique for this element. We can observe a multiple-split for Ni $2p_{3/2}$, which is a typical feature of Ni(II) in NiO, and two high intensity satellites for the two Ni 2p contributions, which are also unique for Ni(II) [45]. Fig. 3d shows the O1s signal. Two peaks are observed: the most intense at a binding energy of 530.1 eV is attributed to the octahedral bond of Ni-O [46], and the peak at a binding energy of 531.8 eV is associated with adsorbed species on the surface of NiO.

FTIR spectrum of the as-prepared NiO nanowires, in powder form, was recorded for confirming the formation of NiO and to analyse the presence of functional groups adsorbed onto surface of NiO. Fig. 3f shows the FTIR spectra for the synthesised sample and a commercial NiO sample for comparison purposes. The FTIR spectrum of the synthesised sample shows peaks at 644 cm^{-1}, 566 cm^{-1} and 526 cm^{-1}, which are assigned to stretching vibrations of Ni-O [47]. The broad band around 3600–3400 cm^{-1} and

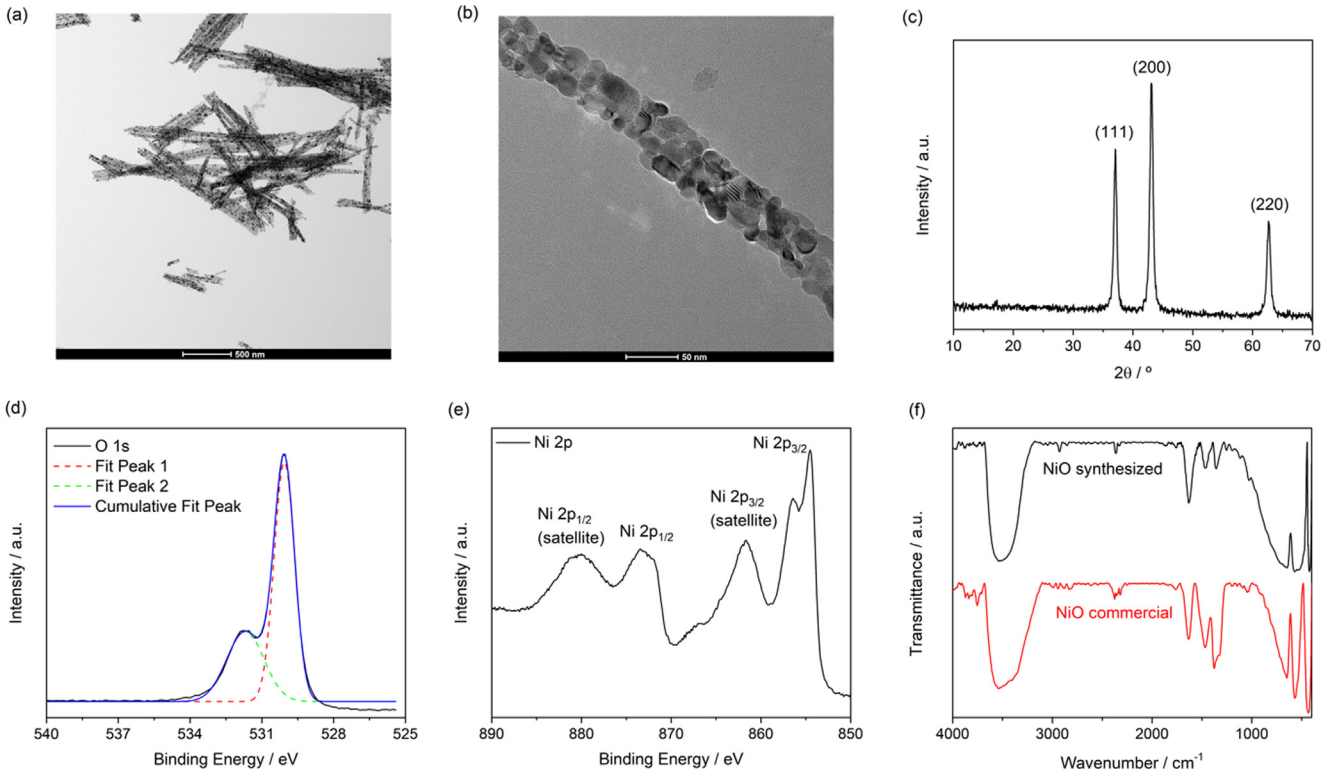

Fig. 3. TEM images (a,b); XRD pattern (c) obtained after annealing process at 500 °C; high-resolution XP spectra for O 1 s (d), and Ni 2p (e) regions; and FTIR spectrum for the NiO nanowires synthesised, and of commercial NiO including for comparison purposes (f).

the one at 1629 cm^{-1} are assigned to O—H stretching vibrations and H—O—H bending vibrations, respectively [48,49]. In addition, several bands are observed in the 1300–1500 cm^{-1} region, which are related to adsorbed species, such as carbonates or water. Particularly, the bands at 1467 cm^{-1} and 1344 cm^{-1} are related to stretching modes of carbonates [50]. Despite the presence these adsorbed species, FTIR spectra confirm NiO nanowires have been successfully produced.

3.2. Colloidal stability of NiO nanowire-containing nanofluids

The as-prepared NiO nanowires were dispersed in the base fluid by sonication, as it was described above. Nanofluids (and colloids, in general) are systems in which the nanomaterial in suspension tends to aggregate, due to attractive forces and, sediment. This is a handicap for its application as HTF, because if the disperse phase collapses, the enhancement in thermal properties is lost. Therefore, the assessment of colloidal stability is a central before evaluating the thermal performance of nanofluids. Here, we will use semi-quantitative evaluation methods to analyse colloidal stability. The particle size was measured in order to determine the tendency of the nanowires to agglomerate. ζ-potential was also measured, as it can be related to the kinetic stability due to repulsion between adjacent particles in suspension [51]. Both variables were measured for more than 6 months after preparation, as shown in Fig. 4. Each point and error bar represent the average and the standard deviation of the daily record. The relative standard deviation in the measurement of particle size and ζ-potential were determined to be better than 2.5% and 7.5%, respectively. The precision of these measurements is exceptionally compromised at some points for well-known reasons: (i) the limited applicability of these techniques (based on the Stoke-Einstein and the Einstein-Smoluchowski equations, respectively) to dispersions of non-spherical particles; (ii) the eventuality of a highly dynamic undergoing aggregation process; and (iii) the need, in the particular case of the ζ-potential, of high voltages to induce electrophoretic mobility of particles in a dispersant phase of very low dielectric constant. For the above stated reasons, the following analysis is considered to be semi-quantitative only.

Fig. 4a shows the particle size of the prepared nanofluids as a function of time. The average particle size as of the day of preparation was determined to be within 235–255 nm, and it gradually increased during the first two weeks after that moment, remaining stable thereafter. The most concentrated nanofluid samples, with NiO contents of 0.01 wt% and 0.001 wt%, reached average particle sizes of 320–340 nm, whereas the sample with a NiO content of 0.0001 wt% reached an average particle size of 290 nm. These values seem not to be change for the rest of the characterisation window, which indicates that the suspension is very stable over time. Particle size remains the same for more than 6 months after of preparation of nanofluids.

The measured ζ-potential values for the same samples are shown in Fig. 4b. High ζ-potential values indicate a high repulsion potential between structures, making aggregation difficult and consequently producing a stable colloidal system [52]. It is precisely during the first two weeks after preparation that the ζ-potential values oscillate more as a consequence of the undergoing aggregation process. Thereafter, ζ-potential values show less variability, indicating that it is from that moment when the nanofluids are stable. These results are in good agreement with the average particle size measurements shown in Fig. 4a.

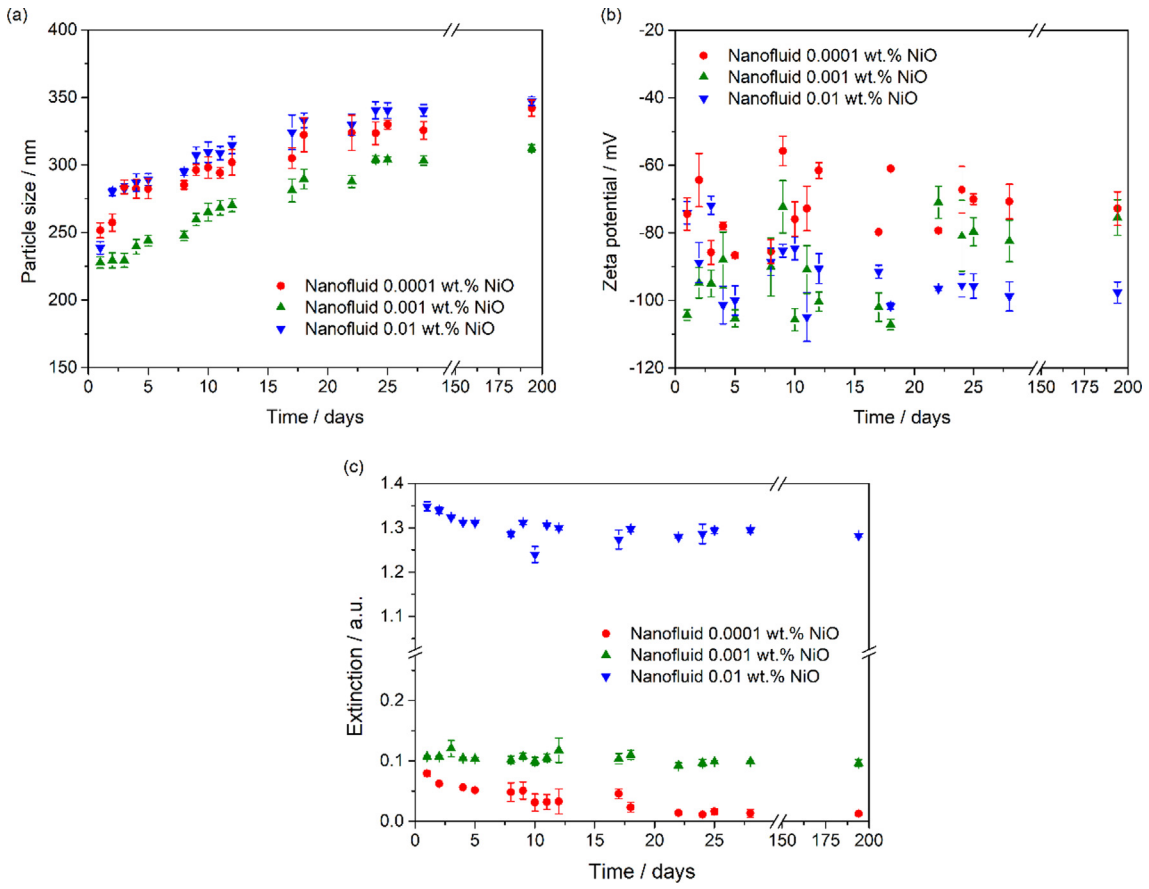

Fig. 4. Particle size (a), ζ-potential (b), and extinction values (c) measured for the nanofluid samples prepared, as a function of time.

The nanofluids were simultaneously monitored by means of UV–visible spectroscopy, as the spectral extinction coefficient is also a good indicator for colloidal stability [53]. Absorbed and scattered radiation is directly proportional to the species in suspension, so that time invariant values of the spectral extinction coefficient indicate good stability. Fig. 4c shows the extinction coefficient at a wavelength of 500 nm for the three nanofluids. A slight decrease in the extinction coefficient values is also observed during the first two weeks after preparation, and it remains stable onwards. Such a decrease is attributed to the aggregation of nanowires, as shown by the results obtained from particle size and ζ-potential measurements.

3.3. Thermal and rheological properties of NiO nanowire-containing nanofluids

Density was measured by pycnometry at 298 K. Five measurements were performed for each sample. The average results are reported in Table 1. The measured value for the base fluid is 1055.7 kg·m^{-3} at 298 K, matching the value provided the supplier at the same temperature [54] and thus proving the accuracy of the measurements. The relative standard deviation of the measurements is better than 1.0%. An increase in the density values was found for all nanofluid samples, with respect to the base fluid, due to the higher density of the NiO. The largest increase was determined to be 2.5%, for the nanofluid with the highest weight fraction of NiO nanowires. Such increase is sufficiently small to consider that density will not play a key role on heat transfer enhancement or affect pumping requirements. The volume fractions of the samples were estimated from density values as $\phi(vol.\%) = 100\hat{A} \cdot \left[\left(\rho_{nf} - \rho_{bf}\right)/\left(\rho_{np} - \rho_{bf}\right)\right]$, where the subscripts *nf*, *bf* and *np* stand for the nanofluid, the base fluid and the nanomaterial (ρ_{np} = 6670 kg m^{-3}), respectively. The volume fractions are also shown in Table 1. The volume fraction serves as indicators for the effective concentration of NiO nanowires in the nanofluid samples by the end of the colloidal stability characterisation.

The rheometric behaviour of the nanofluids prepared was analysed from the measurements of apparent viscosity as a function of the shear rate. Fig. 5a shows rheological profiles of each sample for the whole shear rate range under study. It is determined that the reliable range for measurement [55] for these samples in our rotational rheometer with a concentric cylinder geometry is within 5–25 s^{-1}. At higher shear rates, the flow regime transitions from laminar to turbulent, which compromises the quality of the measurement by introducing an additional bearing friction. This artificially increases the apparent viscosity. A clear turbulent flow regime exists for shear rates over 100 s^{-1}, with sample ejection events. Rheological behaviour in the reliable range is clearly Newtonian. Fig. 5b shows the measured (range-averaged) dynamic viscosity values of the samples as function of temperature. The measured value for the base fluid is 3.59 mPa·s at 298 K, while the value provided by the supplier is 3.64 mPa·s at the same temperature [54]. The relative difference is 1.4%, which demonstrates the accuracy of the measurements. The relative standard deviation of the measurements is better than 1.8%. In addition, we can observe an exponentially decreasing viscosity for increasing temperatures, as it is expected according to the trend reported by the supplier in the technical datasheet of the Dowtherm A HTF. Also, a slight increase in viscosity is observed in nanofluids compared to base fluid, up to 3.3%. Changes in viscosity with respect to the base fluid have been previously reported to be due to nanomaterial-fluid and nanomaterial-nanomaterial interactions and the eventual formation of aggregates in suspension [56]. Given the fact the samples under study have a very low NiO nanowire content, and the fact the no large aggregates are formed according to the stability analysis, it is reasonable to measure such small change in viscosity. This increase can be considered negligible, so that no rheological penalty should be expected for neither heat transfer nor pumping requirements. Thus, no negative impact is expected on the performance of CSP-PTC systems if using these nanofluids.

Regarding thermal properties of the nanofluids, Fig. 6a shows the values of the isobaric specific heat of the nanofluids prepared in function of the volume fraction and temperature. The measured value for the base fluid is 1.614 kJ·kg^{-1}·K^{-1} at 298 K, while the value provided the supplier is 1.587 kJ·kg^{-1}·K^{-1} at the same temperature [54]. The relative difference is 1.7%, which demonstrates the accuracy of the measurements. The relative standard deviation of the measurements is better than 2.0%. We can observe a decrease of the isobaric specific heat for the lowest concentrated nanofluid with respect to the base fluid. Typically, solids have lower isobaric specific heat values than liquids, so nanofluids are typically expected to have lower values than the corresponding base fluid [57,58]. On the other hand, isobaric specific heat does not follow a linear trend as a function of the volume fraction of NiO, as it is observed in Fig. 6a. A relative maximum is found at the intermediate concentration, at all temperatures studied. This behaviour is not explained by the typical models considering nanofluids as a binary system, but the presence of a unique solid–liquid interface can explain these values, as reported by Hentschke [59]. This phenomenological model proposes, as it is supported by previous observations [60–62], that the existence of a physically or chemically adsorbed layer of base fluid molecules on the nanostructure surface is responsible of the enhancement in specific heat, due to the new interactions at the interface. As the volume fraction increases, the interfaces of adjacent nanostructures overlap, and such situation imposes a long-range structural ordering on base fluid molecules, forming a solid-like network of lower specific heat. The observation of such a unique behaviour in the NiO nanowire-containing nanofluids here reported is indirect evidence of the formation of some kind of ordered layer at the interface of these nanofluid. The model is, as previously mentioned, phenomenological, but it has raised the opportunity to study this issue of nanofluids by means of molecular simulations techniques [19,63–65].

In addition, Fig. 6b shows the values of thermal conductivity measured for the base fluid and all nanofluid samples. The measured value for the base fluid is 0.107 W·m^{-1}·K^{-1} at 373 K, while the value provided the supplier is 0.126 W·m^{-1}·K^{-1} at the same temperature [54]. The relative difference is 15%, which demonstrates the accuracy of the measurements. The relative standard deviation of the measurements is better than 6.9% in all cases, and better than 3.5% below 373 K. The effect of natural convection in samples increases the uncertainty of the measurement, which is a known issue of the THB technique [66]. The measured values for the base fluid decrease for increasing temperatures, which is consistent with the values reported by the supplier in its technical datasheet. A change in the trend of the values with temperature is observed for the nanofluids with respect to the base fluid, which has been previously reported for nanofluids prepared using this base fluid [67]. Thermal conductivity of these nanofluids is found to be higher than that of the base fluid over the entire temperature range. The highest increase to be reported is about 100% at 348 K.

Table 1
Density values and volume fraction for the base fluid and the nanofluids prepared.

Sample	ρ / kg m^{-3}	ϕ / vol.%
Base fluid	1055.7 ± 1.1	–
NiO 0.0001 wt%	1057.2 ± 3.0	0.027
NiO 0.001 wt%	1068.6 ± 4.6	0.230
NiO 0.01 wt%	1082.2 ± 7.6	0.472

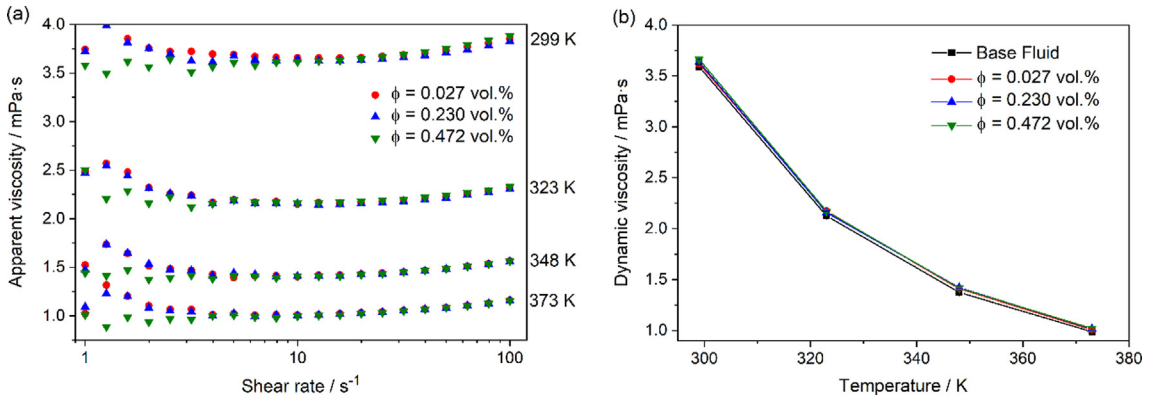

Fig. 5. Viscosity values at different shear rate and temperature for the base fluid and for the nanofluids prepared; (b) dynamic viscosity values at different temperatures. Solid lines do not represent actual data but are included as guide to the eye.

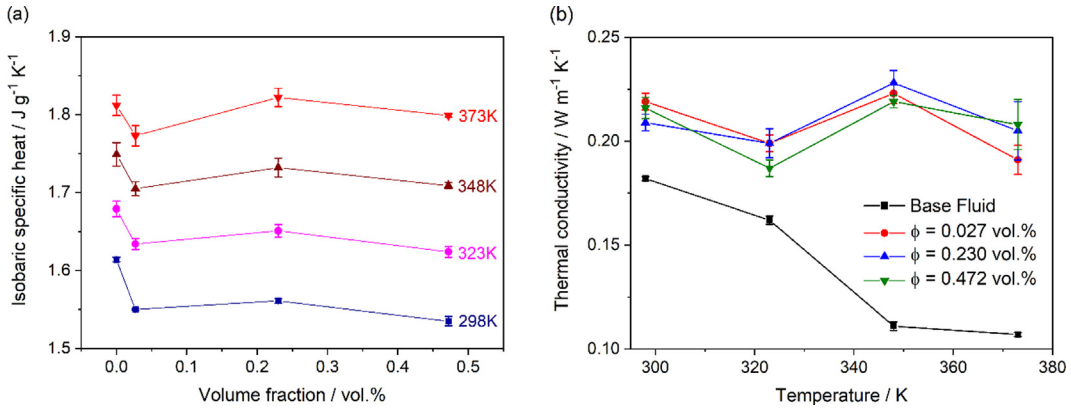

Fig. 6. Isobaric specific heat (a) and thermal conductivity (b) values for the nanofluids prepared in function of the volume fraction and temperature. Solid lines do not represent actual data but are included as guide to the eye.

However, we determined that the THB technique has no sufficient precision to measure a change in thermal conductivity within the range of volume fractions under study. In other words, all three samples are indistinguishable in terms of thermal conductivity, as the thermal conductivity difference between them is no discernible from the experimental uncertainty, but it is clearly observed tht thermal conductivity of these nanofluidos was found to be significantly higher than that of the base fluid.

3.4. Performance of 0.472 vol% NiO nanowire-containing nanofluids as heat transfer fluid and volumetric absorber

The previously presented experimental results are indicative of the applicability of NiO nanowire-containing nanofluid samples to be used as (i) volumetric absorbers, because the dispersion of this nanomaterial in concentrations 0.472 vol% or above is sufficient to promote, by scattering mainly, visible light extinction, and also as (ii) heat transfer fluids, since lower specific heat and significant thermal conductivity enhancements, with very much no change in the rheological profile of the fluid, are found for the same concentration. It all constitutes a set of characteristics that should be assessed at once, by means of existing numerical models, to objectively determine the performance of this nanofluid sample.

In this section we raise a discussion about the design demands for surface and volumetric parabolic-trough collectors in CSP plants, so that the heat transfer fluid (either the typical base fluid or the 0.472 vol% NiO nanofluid) achieves the maximum operating temperature (which is T_{max} = 673 K, for the stability of the Dowtherm A fluid not to be compromised) as it flows through the solar field. The discussion is built on the basis of the expected outlet temperatures for the heat transfer fluid, T_{out}, as a function of the total collector length, L, as plotted in Fig. 7a. The values of T_{out} for both collector types can be estimated using the numerical models proposed by Bellos and Tzivadinis [68] and O'Keeffe et al. [69]. The expressions provided in the original papers (which will be included in the Supplementary Material) are nearly analytical solutions to a steady-state one-dimensional heat transfer problem under turbulent flow regime. Such expressions can be used with no computational cost and parametrised using the optical characteristics, dimensions and flow rate of actual collectors [70–72], and the density, dynamic viscosity, specific heat and thermal conductivity values extrapolated (to any temperatures beyond the operational limit of the characterisation tools) from fitting functions to the experimental datasets reported in this work.

Fig. 7a allows to easily identify the required L for each case to fulfil the $T_{out} = T_{max}$ condition. For the case of a standard surface parabolic-trough collector with either the Dowtherm A heat transfer fluid (solid line) or the 0.472 vol% NiO nanowire nanofluid (dashed line), the T_{out} = 673 K is met at L = 270 m. For the case of a volumetric parabolic-trough collector with the 0.472 vol% NiO nanowire nanofluid (double dot-dashed line) the T_{out} = 673 K is met at L = 280 m. That is equivalent to installing an additional parabolic-trough module from the solar field, which has a directly associated increase in installation costs, although the use of a volumetric collector for direct absorption of sunlight by the nanofluid avoids surface overheating and prevents thermal stress of the receiver and degradation of the absorbing coating, whose lifespan decays exponentially with temperature [73], and that is ultimately translated into a reduction of maintenance costs and a longer life cycle for the plant. No comments are amended to

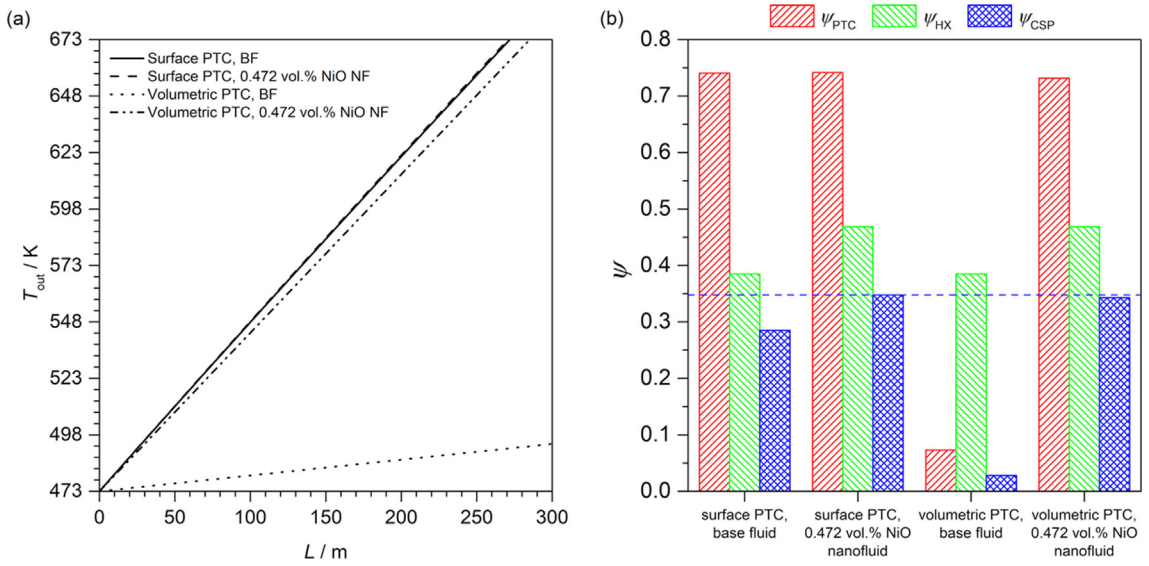

Fig. 7. Outlet temperature T_{out} as a function of the collector length L (a) and collector efficiency Ψ_{PTC}, heat exchanger effectiveness Ψ_{HX} and CSP system performance Ψ_{CSP} (b) for surface and volumetric absorbers with the base fluid and the nanofluid sample as working fluids.

the case of volumetric parabolic-trough collector with the Dowtherm A heat transfer fluid (dotted line), as it is clearly unpractical. Except for the latter, the collector efficiencies, Ψ_{PTC}, which can also be calculated as proposed by Bellos and Tzivadinis [68] and O'Keeffe et al. [69], are found to be very similar in all other cases, with marginal differences below 1%, as shown in Fig. 7b.

As the heat transfer fluid exits the solar field it enters a heat exchanger that takes part into a Rankine vapor cycle. The change in the physical properties of the heat transfer fluid upon dispersion of the nanomaterial also affects the effectiveness of the heat exchanger, Ψ_{HX}, which we have estimated using the number of transfer units (NTU) method (details are provided in the Supplementary Material) and plotted in Fig. 7b. Here, a higher thermal conductivity implies a higher heat transfer rate per unit temperature, and lower specific heat implies a higher NTU for that given heat transfer rate. Such situation is indeed achieved when the 0.472 vol% NiO nanowire nanofluid is considered to be used as heat transfer fluid ($\Psi_{HX,\,nf}$ = 46.9%) over the typical base fluid ($\Psi_{HX,\,bf}$ = 38.5%). This sample, among those under study, provides the lowest specific heat with a negligible small increase in density. More research is needed to evaluate if specific heat could be further decreased by increasing the NiO content in these nanofluids without compromising stability.

As a result, the overall CSP system performance, $\Psi_{CSP} = \Psi_{PTC}\hat{A} \cdot \Psi_{HX}$, as it is shown in Fig. 7b too, can be increased up to 34.8% using the nanofluid in a surface collector or up to 34.3% using the nanofluid in a volumetric collector, which are better than the predicted 28.5% using the Dowtherm A fluid in a standard surface collector. The findings from this assessment should be taken as quantitatively rough but qualitatively significant estimates, and that allows us to safely conclude that the use of NiO nanowires as disperse phase for nanofluids with application not only as heat transfer fluids but also as volumetric absorbers for CSP plants.

3.5. Influence of NiO nanowire crystallinity on the thermal conductivity of nanofluids

The choice of NiO nanowires as a disperse solid phase for nanofluids with application in CSP is not arbitrary but strengthen by a number of reasons. First, NiO has excellent chemical inertia and resistance to thermal degradation, and a bulk thermal conductivity larger than that of the base fluid. Second, the fact that nanowires are, ideally, 1D nanostructured materials, in the sense that only one of his dimensions is not restricted to the nano-scale, which limits the number of phonon–phonon scattering events. That is ultimately translated into longer phonon mean free paths and much higher thermal conductivity than the bulk, as it has been previously discuss by Moreland et al. [17] and Henry et al. [16]. Third and last, this product can be synthesised by a low-cost, straightforward, fast and scalable hydrothermal method, which is the trick of the trade in the formulation of nanofluid for industrial applications like CSP. However, such synthesis method produces polycrystalline NiO nanowires only. The crystallinity of materials, just like their dimensionality, is a key factor on determining is thermal conductivity, as grain boundaries promote phonon scattering and limit heat conduction [18]. The following analysis at the MD level-of-theory aims to assess whether the use of monocrystalline rather than polycrystalline NiO nanowires could further enhance the thermal conductivity of nanofluids upon dispersion, so that the design and optimisation of alternative synthetic schemes can be approached in future studies, without compromising the cost-efficiency of the application.

Fig. 8a compares the Green-Kubo thermal conductivity values from all models under study, and evidences that, even if the thermal conductivity of both nanofluid models are much higher than that of the base fluid, the enhancement is notably larger with a monocrystalline NiO nanowire than with a polycrystalline one. This comparison is intended for qualitative purposes only, as the calculated magnitudes are overestimated by the use of a size-limited simulation cell with an enormous mass fraction of solid, and the lack an *ad hoc* functional of classic potentials for the calculation of thermal conductivity in this particular system. This result is still sufficient to encourage the shaping and sharpening of new and existing synthetic schemes for the production of monocrystalline NiO nanowires, as it proves that there is room for further improvement in the thermal conductivity of heat transfer nanofluids.

From a more fundamental perspective, the difference in the Green-Kubo thermal conductivity between nanofluid models with monocrystalline or polycrystalline nanowires is the result of unequal energy transfer process through these models.

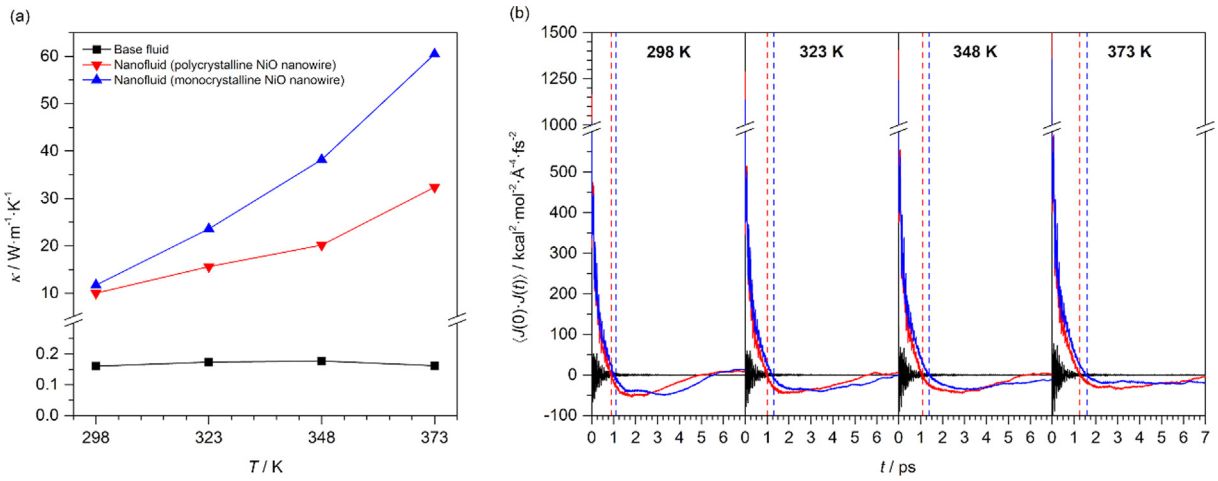

Fig. 8. Green-Kubo thermal conductivity values (a) and heat flux autocorrelation functions (b), as a function of temperature, for the base fluid model and both nanofluid models.

Information about this process can be derived from the heat flux vector auto-correlation function, $\langle \vec{J}(0)\hat{A}\cdot\vec{J}(t)\rangle$, whose integral is directly proportional to thermal conductivity, κ, as given by the following Green-Kubo relation.

$$\kappa = \frac{V}{k_B T^2}\lim_{t\to\infty}\int_0^t \langle \vec{J}(0)\hat{A}\cdot\vec{J}(t)\rangle dt \quad (1)$$

where k_B is the Boltzmann's constant, and T and V are, respectively, the temperature and volume of the simulation cell at equilibrium. In Fig. 8b we compare the $\langle \vec{J}(0)\hat{A}\cdot\vec{J}(t)\rangle$ functions of all three models at each temperature. The $\langle \vec{J}(0)\hat{A}\cdot\vec{J}(t)\rangle$ function features, in all systems, oscillations with frequencies within 10^{13}-10^{14} Hz due to vibrations of C—H, C—C and C—O bonding interactions in base fluid molecules. These oscillations are interpreted as the energy back-and-forth transfer through the system, and their amplitude is damped over time as heat dissipates in the fluid. Damping is critical in the base fluid model but mild in nanofluid models, which means heat is dissipated faster in the base fluid model than in nanofluid models. The long-lasting oscillations in the $\langle \vec{J}(0)\hat{A}\cdot\vec{J}(t)\rangle$ functions of nanofluid models suggests the presence of a NiO nanowire increases the mean free-path of thermal vibrations in the system, even more in presence of a monocrystalline nanowire than in presence of a polycrystalline one, as grain boundaries reduce the mean free-path of thermal vibrations. As temperature increases within the 298–373 K range, so does the time it requires for $\langle \vec{J}(0)\hat{A}\cdot\vec{J}(t)\rangle$ to decay to zero. Numerically, the longer it takes for the $\langle \vec{J}(0)\hat{A}\cdot\vec{J}(t)\rangle$ function to decay to zero, the longer it takes for its integral to saturate, which results into a higher thermal conductivity. It all strengthens the former statement for future approaches for the production of monocrystalline NiO nanowires to be used in heat transfer nanofluids.

4. Conclusions

In this work polycrystalline NiO nanowires-based nanofluids have been prepared using the conventional HTF used in CSP plants as the base fluid. The stability, rheological and thermal properties have been characterised, and an analysis of the performance of the nanofluids prepared in conventional and volumetric absorbers have been performed.

NiO nanowires were synthesised and characterised. From TEM, XRD and XPS, the synthesis of polycrystalline NiO nanowires was confirmed. Nanofluids were prepared using three concentrations of NiO nanowires. The stability of the colloidal suspension was studied by means of particle size, ζ-potential and extinction coefficients measurements. These properties were measured for one month, and measurements after 200 days were performed for analysing the long-term stability. We observe nanofluids reached a good stability several days after preparation. The stable nanofluids were characterised in the properties of interest, that is density, rheological properties, specific heat and thermal conductivity. Density was found to be increased by 2.4%. Also, a slight increase in dynamic viscosity was obtained, up to 3.3%. A Newtonian behaviour was also observed for the nanofluids prepared in the shear range studied. Regarding thermal properties, a significant increase in thermal conductivity was found, reaching a maximum at about 100%, which is a very remarkable value. The values of these properties were used for analysing the performance of the most concentrated nanofluid used as HTF in surface and volumetric absorbers. The overall CSP system performance can be increased up to 34.8% using the nanofluid in a surface collector or up to 34.3% using the nanofluid in a volumetric collector, which are better than the predicted 28.5% using the conventional fluid in a standard surface collector. These findings allow us to safely conclude that the use of NiO nanowires as disperse phase for nanofluids, with application not only as heat transfer fluids but also as volumetric absorbers, would represent a substantial increase in its performance in CSP plants.

Finally, using molecular dynamics simulations, the effect of the crystallinity of the NiO nanowires in the overall thermal conductivity of nanofluids was studied. We found that the mean free path of thermal vibrations is longer for monocrystalline NiO nanowires. Thus, the development of strategies for obtaining this kind of nanostructures is of great interest because they can further improve the efficiency of these nanofluids.

CRediT authorship contribution statement

Desireé M. De los Santos: Conceptualization, Methodology, Investigation, Writing – original draft. **Iván Carrillo-Berdugo:** Conceptualization, Methodology, Investigation, Writing – original draft. **Alejandro Domínguez-Núñez:** Methodology. **Juan Antonio Poce-Fatou:** Formal analysis, Writing – original draft. **David Zorrilla:** Formal analysis. **Javier Navas:** Writing – review & editing, Supervision, Project administration, Funding acquisition.

Declaration of Competing Interest

The authors declare that they have no known competing financial interests or personal relationships that could have appeared to influence the work reported in this paper.

Acknowledgements

I.C.-B. thanks *Ministerio de Universidades del Gobierno de España* for endorsing his postdoctoral position at the University of Cadiz with a *Margarita Salas* fellowship, granted within the call for *Recualificación del* Sistema Universitario Español para 2021-2023, funded by the NextGeneration EU programme of the European Union. We acknowledge Ministerio de Ciencia e Innovación del Gobierno de España for funding under Grant No. RTI2018-096393-B-I00 and for financial support related to measurements of thermal properties, which were carried out using devices acquired under Grant No. UNCA15-CE-2945. Also, this work has been co-financed by the 2014-2020 ERDF Operational Programme and *Consejería de Transformación Económica, Industria, Conocimiento y Universidades de la Junta de Andalucía*, project reference FEDER-UCA18-107510.

Appendix A. Supplementary material

Supplementary Material includes expressions and parameters for the calculation of outlet temperatures and efficiencies of parabolic-trough collectors and the effectiveness of heat exchangers. Supplementary data to this article can be found online at https://doi.org/10.1016/j.molliq.2022.119593.

References

[1] N.H. Md Tasbirul Islam, A. B. Abdullah, R. Saidur. A comprehensive review of state-of-the-art concentrating solar power (CSP) technologies: Current status and research trends, Renewable and Sustainable Energy Reviews 91, 987 (2018). 10.1016/j.rser.2018.04.097.
[2] C.Z. Wang Fuqiang, Tan Jianyu, Yuan Yuan, Shuai Yong, Liu Linhua. Progress in concentratted solar power tecnology with parabolic trough collector system: A comprehensive review, Renew. Sustain. Energy Rev. 79 (2017) 1314, https://doi.org/10.1016/j.rser.2017.05.174.
[3] A.L. Andrea Giglio, Pierluigi Leone, Margarita M. Rodríguez García, Eduardo Zarza Moya. Direct steam generation in parabolic-trough collectors: A review about the technology and a thermo-economic analysis of a hybrid system, Renewable and Sustainable Energy Reviews 74, 453 (2017). http://dx.doi.org/10.1016/j.rser.2017.01.176.
[4] S.N. Kevin Coscia, T. Elliott, S. Mohapatra, Alparslan Oztekin, Sudhakar Neti. Thermophysical Properties of $LiNO_3$-$NaNO_3$-KNO_3 Mixtures for Use in Concentrated Solar Power, J. Sol. Energy Eng. 135 (2013) 1, https://doi.org/10.1115/1.4024069.
[5] P. Good, G. Ambrosetti, A. Pedretti, A. Steinfeld, 1.2 MWth solar parabolic trough system based on air as heat transfer fluid at 500 °C - Engineering design, modelling, construction, and testing, Sol. Energy 139 (2016) 398–411.
[6] E. Bellos, C. Tzivanidis, K.A. Antonopoulos, A detailed working fluid investigation for solar parabolic trough collectors, Appl. Therm. Eng. 114 (2017) 374–386.
[7] E.Z. Moya. Innovative working fluids for parabolic trough collectors, in Advances in Concentrating Solar Thermal Research and Technology, 75-106, (2017). 10.1016/B978-0-08-100516-3.00005-8.
[8] N. Abed, I. Afgan, An extensive review of various technologies for enhancing the thermal and optical performances of parabolic trough collectors, Int. J. Energy Res. 44 (7) (2020) 5117–5164.
[9] L.M.G. Elena, A. Chernikova, V.G. Krasovskiy, L.M. Kustov, M.G. Vorobyeva, A.A. Koroteev, Ionic liquids as heat transfer fluids: comparison with known systems, possible applications, advantages and disadvantages, Russ. Chem. Rev. 84 (2015) 875, https://doi.org/10.1070/RCR4510.
[10] M.F. Yathin Krishna, R. Saidur, K.C. Ng, Navid Aslfattahi. State-of-the-art heat transfer fluids fr parablic trough collector, Int. J. Heat Mass Transf. 152 (2020) 1, https://doi.org/10.1016/j.ijheatmasstransfer.2020.119541.
[11] R.M. J. Sunil, R. Vettumperumal, and Kishor Kumar Sadasivuni. Experimental Investigation on the Thermal Properties of NiO-Nanofluids, Journal of Nanofluids 8, 1577 (2019). 10.1166/jon.2019.1698
[12] A.A.P. Poppy Puspitasari, Maizatul Shima Shaharun, and Dewi Izzatus Tsamroh. Heat transfer characterisctics of NiO nanofluid in heat exchanger, AIP Conf. Proc. (2020) 9, https://doi.org/10.1063/5.0000883.
[13] E.I.M. Antonio Sánchez-Coronilla, Javier Navas, Teresa Aguilar, Roberto Gómez-Villarejo, Rodrigo Alcántara, Jose Carlos Piñero, Concha Fernández-Lorenzo. Experimental and theoretical analysis of NiO nanofluids in presence of surfactants, Journal of Molecular Liquids 252, 211 (2018). 10.1016/j.molliq.2017.12.140.
[14] J.N. Teresa Aguilar, Antonio Sánchez-Coronilla, Elisa I. Martín, Juan Jesús Gallardo, Paloma Martínez-Merino, Roberto Gómez-Villarejo, José Carlos Piñero, Rodrigo Alcántara, Concha Fernández-Lorenzo. Investigation of enhanced thermal properties in NiO-based nanofluids for concentrating solar power applications: A molecular dynamics and experimental analysis, Applied Energy 211, 677 (2018). 10.1016/j.apenergy.2017.11.069.
[15] T.T.L. Dang, M. Tonezzer, Polycrystalline NiO Nanowires: Scalable Growth and Ethanol Sensing, Procedia Eng. 120 (2015) 427.
[16] A. Henry, G. Chen, S.J. Plimpton, A. Thompson, 1D-to-3D transition of phonon heat conduction in polyethylene using molecular dynamics simulations, Phys. Rev. B 82 (2010) 1, https://doi.org/10.1103/PhysRevB.82.144308, 144308.
[17] J.F. Moreland, J.B. Freund, G. Chen, The disparate thermal conductivity of carbon nanotubes and diamond nanowires studied by atomistic simulation, Microscale Thermophys. Eng. 8 (2004) 61, https://doi.org/10.1080/10893950490272939.
[18] H. Dong, B. Wen, R. Melnik, Relative importance of grain boundaries and size effects in thermal conductivity of nanocrystalline materials, Sci. Rep. 4, 7037 (2014) 1, https://doi.org/10.1038/srep07037.
[19] I. Carrillo-Berdugo, R. Grau-Crespo, D. Zorrilla, J. Navas, Interfacial molecular layering enhances specific heat of nanofluids: evidence from molecular dynamics, J. Mol. Liq. 325 (2021) 115217.
[20] W.L. Jorgensen, J. Tirado-Rives, The OPLS [Optimized Potentials for liquids simulation] potential functions for proteins, energy minimizations for crystals of cyclic peptides and crambin, J. Am. Chem. Soc. 110 (1988) 1657, https://doi.org/10.1021/ja00214a001.
[21] W.L. Jorgensen, D.S. Maxwell, J. Tirado-Rives, Development and testing of the OPLS all-atom force field on conformational energetics and properties of organic liquids, J. Am. Chem. Soc. 118 (1996) 11225, https://doi.org/10.1021/ja9621760.
[22] W.L. Jorgensen, J. Tirado-Rives, Potential energy functions for atomic-level simulations of water and organic and biomolecular systems, Proc. Natl. Acad. Sci. U.S.A. 102 (2005) 6665, https://doi.org/10.1073/pnas.0408037102.
[23] L.S. Dodda, J.Z. Vilseck, J. Tirado-Rives, W.L. Jorgensen, 1.14*CM1A-LBCC: localized bond-charge corrected CM1A charges for condensed-phase simulations, J. Phys. Chem. B 121 (2017) 3864, https://doi.org/10.1021/acs.jpcb.7b00272.
[24] L.S. Dodda, I. Cabeza de Vaca, J. Tirado-Rives, W.L. Jorgensen, LigParGen web server: an automatic OPLS-AA parameter generator for organic ligands, Nucleic Acids Res. 45 (2017) 331, https://doi.org/10.1093/nar/gkx312.
[25] L. Zhao, L. Liu, H. Sun, Semi-ionic model for metal oxides and their interfaces with organic molecules, J. Phys. Chem. C 111 (2007) 10610, https://doi.org/10.1021/jp071775y.
[26] J.D. Gale, A.L. Rohl, The general utility lattice program (GULP), Mol. Simul. 29 (2003) 291, https://doi.org/10.1080/0892702031000104887.
[27] J.D. Gale. General Utility Lattice Program (GULP), 5.1.1 (2019). http://gulp.curtin.edu.au/gulp/.
[28] J.D. Gale, Gulp,, A Computer program for the symmetry-adapted simulation of solids, J. Chem. Soc., Faraday Trans. 93 (1997) 629, https://doi.org/10.1039/A606455H.
[29] J.D. Gale, GULP: capabilities and prospects, Z. Krist. 220 (2005) 552, https://doi.org/10.1524/zkri.220.5.552.65070.
[30] A. Arkundato, F. Monado, Supeno, Misto, Z. Su'ud. Performance of the Fe-Ni-Cr steel alloy in high temperature molten liquid lead, J. Phys.: Conf. Ser. 1170, 012010, 1 (2019). 10.1088/1742-6596/1170/1/012010.
[31] S. Plimpton, Fast parallel algorithms for short-range molecular dynamics, J. Comput. Phys. 117 (1) (1995) 1–19.
[32] A.P. Thompson, H.M. Aktulga, R. Berger, D.S. Bolintineanu, W.M. Brown, P.S. Crozier, P.J. in't Veld, A. Kohlmeyer, S.G. Moore, T.D. Nguyen, T. Shan, M.J. Stevens, J. Tranchida, C. Trott, S.J. Plimpton, LAMMPS - a flexible simulation tool for particle-based materials modeling at the atomic, meso, and continuum scales, Comp. Phys. Comm. 271 (2022) 10817, https://doi.org/10.1016/j.cpc.2021.108171.
[33] S. Plimpton, A. Thompson, S. Moore, A. Kohlmeyer, R. Berger. Large Atomic/Molecular Massively Parallel Simulator (LAMMPS), 17Nov2016 (2016). http://lammps.sandia.gov.
[34] A.I. Jewett, Z. Zhuang, J.-E. Shea, Moltemplate a coarse-grained model assembly tool, Biophys. J. 104 (2013) 169a, https://doi.org/10.1016/j.bpj.2012.11.953.
[35] A. Jewett. Moltemplate, 1.34 (2015). https://www.moltemplate.org.
[36] L. Verlet, Computer "experiments" on classical fluids. I. thermodynamical properties of lennard-jones molecules, Phys. Rev. A 159 (1) (1967) 98–103.
[37] S. Nosé, A Molecular dynamics method for simulations in the canonical ensemble, Mol. Phys. 52 (2) (1984) 255–268.
[38] S. Nosé, A unified formulation of the constant temperature molecular dynamics methods, J. Chem. Phys. 81 (1) (1984) 511–519.
[39] W.G. Hoover, Canonical dynamics: equilibrium phase-space distributions, Phys. Rev. A 1985 (1985) 1695, https://doi.org/10.1103/PhysRevA.31.1695.
[40] W.G. Hoover, Constant-pressure equations of motion, Phys. Rev. A 34 (3) (1986) 2499–2500.
[41] M.S. Green, Markoff random processes and the statistical mechanics of time-dependent phenomena. II. irreversible processes in fluids, J. Chem. Phys. 22 (1954) 398, https://doi.org/10.1063/1.1740082.

[42] R. Kubo, Statistical-mechanical theory of irreversible processes. I. general theory and simple applications to magnetic and conduction problems, J. Phys. Soc. Jpn. 12 (6) (1957) 570–586.
[43] D. Wu, L. Zhang, J. Zhang, Z. Zhang, F. Liang, L. Jiang, B. Tang, Y. Rui, F. Liu, Novel self-supporting multilevel-3D porous NiO nanowires with metal-organic gel coating via "like dissolves like" to trigger high-performance binder-free lithium-ion batteries, Microporous Mesoporous Mater. 328 (2021), https://doi.org/10.1016/j.micromeso.2021.111483 111483.
[44] R. Bajaj, A.S. Rao, G.V. Prakash, Linear and nonlinear photoluminescence from thermally stable KYF4:Eu3+ cubic nanocrystals, J. Alloy. Compd. 885 (2021), https://doi.org/10.1016/j.jallcom.2021.160893 160893.
[45] T. Montoya, A. Amrollahi, G. Vitale, N. Hosseinpour, N.N. Nassar, Size Effects of NiO nanoparticles on the competitive adsorption of quinolin-65 and Violanthrone-79: implications for Oil upgrading and recovery, ACS Appl. Nano Mater. 3 (2020) 5311, https://doi.org/10.1021/acsanm.0c00697.
[46] K. Chandra Sekhar Reddy, P. Sahatiya, I. Santos-Sauceda, O. Cortázar, R. Ramírez-Bon, One-step fabrication of 1D p-NiO nanowire/n-Si heterojunction: development of self-powered ultraviolet photodetector, Appl. Surf. Sci. 513 (2020), https://doi.org/10.1016/j.apsusc.2020.145804.
[47] K. Kaviyarasu, E. Manikandan, J. Kennedy, M. Jayachandran, R. Ladchumananandasiivam, U.U. De Gomes, M. Maaza, Synthesis and characterization studies of NiO nanorods for enhancing solar cell efficiency using photon upconversion materials, Ceram. Int. 42 (2016) 8385, https://doi.org/10.1016/j.ceramint.2016.02.054.
[48] P.K. Sharma, M.K. Singh, G.D. Sharma, A. Agrawal, NiO nanoparticles: Facile route synthesis, characterization and potential towards third generation solar cell, Mater. Today:. Proc. 43 (2021) 3061, https://doi.org/10.1016/j.matpr.2021.01.400.
[49] H.T. Handal, W.A.A. Mohamed, A.A. Labib, S.A. Moustafa, A.A. Sery, The influence of surface modification on the optical and capacitive properties of NiO nanoparticles synthesized via surfactant-assisted coprecipitation, J. Storage Mater. 44 (2021), https://doi.org/10.1016/j.est.2021.103321 103321.
[50] H. Bekhti, Y. Boucheffa, A.H.A. Blal, A. Travert, In situ FTIR investigation of CO2 adsorption over MgO–Impregnated NaY zeolites, Vib. Spectrosc. 117 (2021), https://doi.org/10.1016/j.vibspec.2021.103313 103313.
[51] A. Sánchez-Coronilla, E.I. Martín, J. Navas, T. Aguilar, R. Gómez-Villarejo, R. Alcántara, J.C. Piñero, C. Fernández-Lorenzo, Experimental and theoretical analysis of NiO nanofluids in presence of surfactants, J. Mol. Liq. 252 (2018) 211, https://doi.org/10.1016/j.molliq.2017.12.140.
[52] M. Teruel, T. Aguilar, P. Martínez-Merino, I. Carrillo-Berdugo, J.J. Gallardo-Bernal, R. Gómez-Villarejo, R. Alcántara, C. Fernández-Lorenzo, J. Navas, 2D MoSe2-based nanofluids prepared by liquid phase exfoliation for heat transfer applications in concentrating solar power, Sol. Energy Mater. Sol. Cells 200 (2019), https://doi.org/10.1016/j.solmat.2019.109972 109972.
[53] W. Mäntele, E. Deniz, UV–VIS absorption spectroscopy: Lambert-Beer reloaded, Spectrochim. Acta Part A Mol. Biomol. Spectrosc. 173 (2017) 965, https://doi.org/10.1016/j.saa.2016.09.037.
[54] H.t. fluid. Product Technical Data. VLL0-V0100-MA-001. 1997, Company TD. Dowtherm A.,
[55] M. Laun, D. Auhl, R. Brummer, D.J. Dijkstra, C. Gabriel, M.A. Mangnus, M. Rüllmann, W. Zoetelief, U.A. Handge, Guidelines for checking performance and verifying accuracy of rotational rheometers: viscosity measurements in steady and oscillatory shear (IUPAC Technical Report), Pure Appl. Chem. 86 (2014) 1945, https://doi.org/10.1515/pac-2013-0601.
[56] R.D. Selvakumar, S. Dhinakaran, Effective viscosity of nanofluids — a modified krieger-dougherty model based on particle size distribution (PSD) analysis, J. Mol. Liq. 225 (2017) 20, https://doi.org/10.1016/j.molliq.2016.10.137.
[57] D. Cabaleiro, C. Gracia-Fernández, J.L. Legido, L. Lugo, Specific heat of metal oxide nanofluids at high concentrations for heat transfer, Int. J. Heat Mass Transf. 88 (2015) 872–879.
[58] N.S. Susan Mousavi, S. Kumar, Effective heat capacity of ferrofluids - Analytical approach, Int. J. Therm. Sci. 84 (2014) 267–274.
[59] R. Hentschke, On the specific heat capacity enhancement in nanofluids, Nanoscale res. lett. 11 (2016) 88.
[60] D. Shin, D. Banerjee, Enhancement of specific heat capacity of high-temperature silica-nanofluids synthesized in alkali chloride salt eutectics for solar thermal-energy storage applications, Int. J. Heat Mass Transfer 54 (2011) 1064, https://doi.org/10.1016/j.ijheatmasstransfer.2010.11.017.
[61] P. Heilmann, Evaluation, Neuentwicklung und Optimierung des Eigenschaftsprofils von Salzschmelzen für die Verwendung als Wärmeträgerfluide. Bergische Universität: Wuppertal, Germany, 2013; Vol. PhD.
[62] M. Lasfargues, Q. Geng, H. Cao, Y. Ding, Mechanical dispersion of nanoparticles and its effect on the specific heat capacity of impure binary nitrate salt mixtures, Nanomaterials 5 (3) (2015) 1136–1146.
[63] I. Carrillo-Berdugo, R. Grau-Crespo, D. Zorrilla, J. Navas, Interfacial molecular layering enhances specific heat of nanofluids: evidence from molecular dynamics, J. Mol. Liq. 325, 115217 (2020) 1, https://doi.org/10.1016/j.molliq.2020.115217.
[64] E. Leonardi, A. Floris, S. Bose, B. D'Anguanno, Unified description of the specific heat of ionic bulk materials containing nanoparticles, ACS Nano 15 (2021) 563, https://doi.org/10.1021/acsnano.0c05892.
[65] Z. Li, L. Cui, B. Li, X. Du, Mechanism exploration of the enhancement of thermal energy storage in molten salt nanofluid, Phys. Chem. Chem. Phys. 23 (2021) 13181, https://doi.org/10.1039/D1CP00125F.
[66] H.M. Roder, R.A. Perkins, A. Laesecke, C.A. Nieto de Castro, Absolute steady-state thermal conductivity measurements by use of a transient hot-wire system, J. Res. Natl. Inst. Stand. Technol. 10 (2000) 221, https://doi.org/10.6028/jres.105.028.
[67] R. Gomez-Villarejo, J. Navas, E.I. Martín, A. Sánchez-Coronilla, T. Aguilar, J.J. Gallardo, D.D.l. Santos, R. Alcántara, C. Fernández-Lorenzo, J. Martín-Calleja, Preparation of Au nanoparticles in a non-polar medium: obtaining high-efficiency nanofluids for concentrating solar power. An experimental and theoretical perspective, J. Mater. Chem. A 5 (2017) 12483, https://doi.org/10.1039/c7ta00986k.
[68] E. Bellos, C. Tzivanidis, Analytical expression of parabolic trough solar collector performance, Designs 2, 9 (2018) 1, https://doi.org/10.3390/designs2010009.
[69] G.J. O'Keeffee, S.L. Mitchell, T.G. Myers, V. Cregan, Modelling the efficiency of a nanofluid-based direct absorption parabolic trough solar collector, Sol. Energy 159 (2018) 44, https://doi.org/10.1016/j.solener.2017.10.066.
[70] J.C.C. Fan, F.J. Bachner, Transparent heat mirrors for solar energy applications, Appl. Opt. 15 (1976) 1012, https://doi.org/10.1364/AO.15.001012.
[71] V.E. Dudley, G.J. Kolb, A.R. Mahoney, T.R. Mancini, C.W. Matthews, M. Sloan, D. Kearney. Test Results: SEGS LS-2 Solar Collector (Sandia National Laboratories, USA, 1994).
[72] R. Forristal. Heat Transfer Analysis and Modeling of a Parabolic Trough Solar Receiver Implemented in Engineering Equation Solver (NERL, USA, 2003).
[73] O. Raccurt, F. Matino, A. Disdier, J. Braillon, A. Stollo, D. Bourdon, A. Maccari. In Air Durability Study of Solar Selective Coating for Parabolic Trough Technology, AIP Conf. Proc. 1850, 130010, 1 (2017). 10.1063/1.4984504.